





## Emergence of gaussianity in the thermodynamic limit of interacting fermions

Gabriel Matos, Andrew Hallam , Aydin Deger , Zlatko Papić , and Jiannis K. Pachos  
*School of Physics and Astronomy, University of Leeds, Leeds LS2 9JT, United Kingdom*

 (Received 20 July 2021; accepted 25 October 2021; published 19 November 2021)

Systems of interacting fermions can give rise to ground states whose correlations become effectively free-fermion-like in the thermodynamic limit, as shown by Baxter for a class of integrable models that include the one-dimensional XYZ spin- $\frac{1}{2}$  chain. Here, we quantitatively analyze this behavior by establishing the relation between system size and correlation length required for the fermionic gaussianity to emerge. Importantly, we demonstrate that this behavior can be observed through the applicability of Wick's theorem, and thus, it is experimentally accessible. To establish the relevance of our results to possible experimental realizations of XYZ-related models, we demonstrate that the emergent gaussianity is insensitive to weak variations in the range of interactions, coupling inhomogeneities, and local random potentials.

DOI: [10.1103/PhysRevB.104.L180408](https://doi.org/10.1103/PhysRevB.104.L180408)

*Introduction.* Free-particle systems enjoy a privileged place in physics: all of their correlations can be broken down into products of two-point functions, illustrating the computational power of Wick's theorem [1] and greatly aiding their theoretical understanding. This “Gaussian” description can be radically altered in real systems in which interactions are invariably present, leading to exotic interaction-driven phenomena such as fractionalized excitations and topological order [2,3]. At the same time, there are many known examples, e.g., Luttinger liquids [4], for which interactions give rise to new collective degrees of freedom; however, the latter can still be described as being nearly free. It is thus important to have a more systematic understanding of the criteria when interactions can engender nontrivial physical behavior.

In recent years significant attention has been focused on many-body systems that are expected to be strongly interacting yet behave in an approximately Gaussian manner. Recent experiments [5] have shown that Gaussian behavior can emerge *dynamically* as the system is taken out of its equilibrium state. On the other hand, gaussianity can also emerge in *equilibrium*, as the *size* of the system grows infinite. The latter occurs in a one-dimensional (1D) spin- $\frac{1}{2}$  XYZ model, which hosts a variety of paradigmatic models, such as the Heisenberg model, the XY model, and the Ising model, as special cases. In 1970, Sutherland observed that the transfer matrix of the eight-vertex model has the same eigenvectors as the XYZ model [6]. With the help of this mapping Baxter famously solved the 2D classical XYZ model exactly. In particular, he demonstrated that in the thermodynamic limit its partition function can be described by noninteracting fermions throughout its entire phase diagram [7–10]. With the mapping between 2D classical systems and quantum chains [11–13] it was possible to determine the entanglement spectra of the 1D spin- $\frac{1}{2}$  XYZ model directly from Baxter's results [1,14]. Subsequently, the Gaussian structure of the entanglement spectra of the XYZ chain was verified numerically [15].

In this Letter, we propose using the violation of Wick's theorem to measure the fermionic gaussianity emerging in the

XYZ model and its generalizations to long-range spin-spin interactions. When applied to a free-fermion system, Wick's theorem decomposes high-point correlators in terms of two-point correlators [16]. When the system is interacting, this decomposition is not possible, leaving a difference  $\mathcal{W}$  that can be used to quantify the effect of interactions. This approach makes it possible to demonstrate the emergent freedom of a many-body quantum system using simple, physical observables. However,  $\mathcal{W}$  is dependent on the choice of the operator used for Wick's decomposition and therefore needs an upper bound to be physically useful. We demonstrate the efficacy of Wick's theorem by bounding it with the more general diagnostic of gaussianity—the so-called *interaction distance*  $D_{\mathcal{F}}$  [17–19]. Comparing the behavior of both  $D_{\mathcal{F}}$  and  $\mathcal{W}$ , we demonstrate that quantum correlations of the XYZ model exponentially approach those of a free-fermion model as a function of system size, provided the size of the system is larger than the correlation length. For smaller system sizes, the XYZ model appears to be strongly interacting in terms of both Wick's theorem and  $D_{\mathcal{F}}$  near its critical regions, in stark contrast to its thermodynamic limit behavior. To demonstrate the experimental relevance of our results, we analyze the applicability of Wick's theorem in the presence of realistic conditions such as variations in the range of interactions, coupling inhomogeneities, and local random potentials.

*The XYZ model and its emergent freedom.* The 1D spin- $\frac{1}{2}$  XYZ model on an open chain with  $L$  sites is given by

$$H = \sum_i J_x X_i X_{i+1} + J_y Y_i Y_{i+1} + J_z Z_i Z_{i+1}, \quad (1)$$

where  $X_i$ ,  $Y_i$ , and  $Z_i$  are the usual Pauli matrices on site  $i$ . By employing the Jordan-Wigner transformation, the spin model maps to interacting spinless fermions,

$$H = \sum_i J_+ c_i c_{i+1}^\dagger + J_- c_i c_{i+1} + \text{H.c.} + \frac{J_z}{4} n_i n_{i+1} - \frac{J_z}{2} n_i, \quad (2)$$

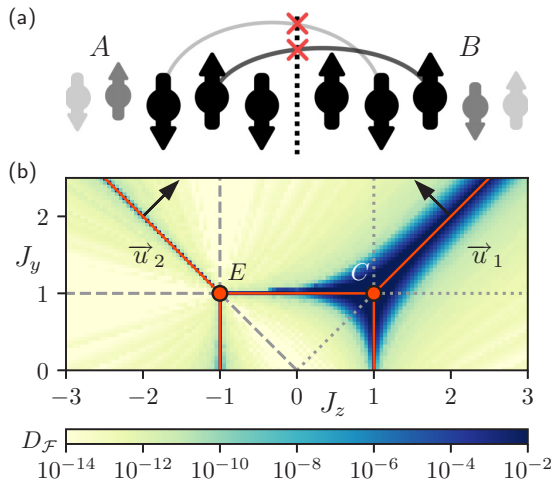


FIG. 1. (a) Quantum correlations across the bipartition (dashed line) of a spin chain. (b) Interaction distance  $D_{\mathcal{F}}$  in Eq. (3), obtained using DMRG across the phase diagram of the XYZ model for  $L = 200$  spins. Red lines denote critical lines, and the conformal (C) and nonconformal (E) tricritical points are indicated [21]. Vectors  $\vec{u}_1$  and  $\vec{u}_2$  are orthogonal to the critical lines and are used in Fig. 2. The interaction distance is strongly suppressed in gapped phases of the XYZ model, signaling the emergence of gaussianity.

where  $J_{\pm} = (J_x \pm J_y)$  and  $n_i = c_i^{\dagger} c_i$ . In the fermionic representation  $J_z$  becomes the interaction coupling between fermion populations at neighboring sites [20]. Without loss of generality we take  $J_x = 1$ , and due to the symmetries  $(J_y, J_z) \leftrightarrow (-J_z, -J_y)$  and  $(J_y, J_z) \leftrightarrow (J_z, J_y)$  of the Hamiltonian, we restrict ourselves to  $J_y \geq 0$ .

To analyze quantum correlations in the ground state of the model  $|\psi_{\text{GS}}\rangle$ , we take the reduced-density matrix of the half chain,  $\rho_A = \text{tr}_B |\psi_{\text{GS}}\rangle\langle\psi_{\text{GS}}|$ , illustrated in Fig. 1(a). The eigenvalues  $\rho_i$  of  $\rho_A$  and the corresponding entanglement energies,  $E_i^{\text{ent}} = -\ln \rho_i$ , contain all information about quantum correlations between the two halves of the chain [22]. The total number of correlations can be quantified by the von Neumann entropy  $S(\rho_A) = -\sum_i \rho_i \ln \rho_i$ . On the other hand, the interaction distance  $D_{\mathcal{F}}(\rho_A)$  diagnoses how close the quantum correlations between the two halves are to those of a Gaussian fermionic state [17]. The interaction distance is defined as

$$D_{\mathcal{F}}(\rho_A) = \min_{\{\epsilon\}} \frac{1}{2} \sum_i |\rho_i - \sigma_i(\epsilon)|, \quad (3)$$

where  $\sigma_i(\epsilon)$  are the eigenvalues of the density matrix  $\sigma(\epsilon)$  of a free model given by  $\sigma_i(\epsilon) = e^{-E_i^{\text{free}}(\epsilon)}$  with entanglement spectrum  $E_i^{\text{free}}(\epsilon) = E_0 + \sum_j \epsilon_j n_j^{(i)}$ , where  $E_0$  ensures the normalization condition  $\text{tr}(\sigma) = 1$ ,  $\epsilon_j$  are the single-particle energies, and  $n_j^{(i)}$  is the occupancy number on the  $j$ th site of the  $i$ th element of the Fock basis, labeled by the index  $i$ . The minimization over the single-particle energies  $\epsilon$  guarantees that  $\sigma$  is the free density matrix which is closest to the interacting  $\rho$  [23]. When  $D_{\mathcal{F}} \rightarrow 0$ , the ground state of the model exhibits Gaussian correlations across the bipartition and can be faithfully described by a free-fermion density matrix  $\sigma$ .

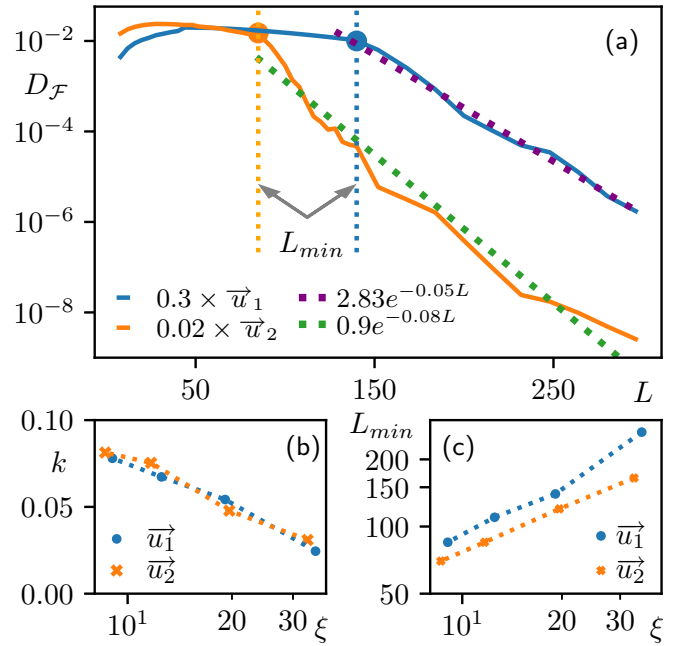


FIG. 2. (a) Exponential decay of  $D_{\mathcal{F}}$  with system size at different points along the  $\vec{u}_1$  and  $\vec{u}_2$  cuts through the phase diagram in Fig. 1. We observe a short initial increase, followed by a plateau and the final decrease beyond some crossover length scale  $L_{\text{min}}$ , indicated by the dotted lines. Dashed lines are fits to the asymptotic exponential decay,  $D_{\mathcal{F}} \propto \exp(-kL)$ , for data points  $L > L_{\text{min}}$ . (b) The slope  $k$  of the exponential decay, extracted at various points along  $\vec{u}_1$  and  $\vec{u}_2$ , exhibits a power-law dependence on correlation length  $\xi$ . The latter is computed using the analytic formulas applicable in the thermodynamic limit [26]. (c) The correlation length  $\xi$  displays power-law dependence on  $L_{\text{min}}$ .

The interaction distance for the XYZ model in Eq. (1), shown in Fig. 1(b), is computed across the phase diagram using the density matrix renormalization group (DMRG) [24], implemented in ITENSOR [25]. Along the line  $J_y = J_z$ , which is equivalent to the XXZ model with antiferromagnetic couplings studied in Ref. [19],  $D_{\mathcal{F}}$  is high around the gapless critical phase  $|J_y| > 1$ . On the line  $J_y = -J_z$ ,  $D_{\mathcal{F}}$  is high across a much narrower region around its  $|J_y| > 1$  gapless phase. Away from the critical regions,  $D_{\mathcal{F}}$  tends to zero, showing that the system exhibits Gaussian correlations. Hence, we will focus our investigation around these gapless regions where  $D_{\mathcal{F}}$  exhibits nontrivial behavior.

Baxter proved that the XYZ model becomes free when  $L \rightarrow \infty$ , provided the correlation length is finite. However, physically, we expect the model to become free as soon as  $L$  exceeds the correlation length  $\xi$ . When applied to the XYZ model, the interaction distance can diagnose the emergence of freedom and thus quantify Baxter's result for various system sizes  $L$  compared to  $\xi$ . Without loss of generality, we consider the behavior of  $D_{\mathcal{F}}$  along  $\vec{u}_1$  cut across the  $J_y = J_z$  critical region and  $\vec{u}_2$ , which crosses the  $J_y = -J_z$  critical region, as shown in Fig. 2(b). We find that, for values of the couplings away from the critical lines,  $D_{\mathcal{F}}$  tends to zero exponentially fast as system size increases, as shown in Fig. 2(a), signaling that the emerging freedom can be observed efficiently. We emphasize that this happens even for large values of the

coupling  $J_z$  that correspond to strong density-density interactions between fermions.

To analyze the conditions under which the system becomes free, we determine the system size  $L_{\min}$  beyond which the interaction distance starts decreasing as well as the rate  $k$  at which  $D_{\mathcal{F}}$  exponentially approaches zero,  $D_{\mathcal{F}} \propto \exp(-kL)$ . Figure 2(b) shows that the rate  $k$  decreases as correlation length  $\xi$  increases; that is, the rate of exponential decay of  $D_{\mathcal{F}}$  decreases the closer we are to the critical regions. Hence,  $D_{\mathcal{F}}$  quantifies Baxter's assumption, showing the quantum correlations of the XYZ model become free-fermion-like by having  $D_{\mathcal{F}} \rightarrow 0$  exponentially fast with  $L$ , provided that the size is larger than a minimum value  $L_{\min}$ . The latter is a polynomial function of the correlation length  $\xi$  [26], as can be seen in Fig. 2(c). We observe that the larger the correlation length is, i.e., the closer to criticality, the larger the system needs to be in order for the interaction distance to exhibit the exponential decay. The observed polynomial relation between  $L_{\min}$  and  $\xi$  quantifies Baxter's assumption for identifying the freedom of the XYZ model [9]. We emphasize that this strong dependence of  $D_{\mathcal{F}}$  on  $L$  allows us to efficiently identify the emergent gaussianity in a quantum simulation of the XYZ model with an exponential accuracy just with a linear cost in the size of the simulated system.

*Violation of Wick's theorem and experimental implications.* Investigating the behavior of the XYZ model in terms of the interaction distance reveals its formal emergence of gaussianity in a quantitative way. Ideally, we would like to have an experimentally accessible quantity that would allow us to measure the emergent freedom in the laboratory. In general, the full entanglement spectrum of the system can be difficult to extract in an experimental context [27–29]. We therefore turn to the violation of Wick's theorem due to interactions.

Definition (3) allows us to determine the optimal free state  $\sigma$  closest to  $\rho$ . Moreover, they are both diagonal in the same basis [17] that can be expressed in terms of the eigenoperators  $a_j$  and  $a_j^\dagger$ . When  $\rho$  corresponds to a Gaussian state, Wick's theorem dictates that  $\langle a_i^\dagger a_i a_j^\dagger a_j \rangle_\rho = \langle a_i^\dagger a_i \rangle_\rho \langle a_j^\dagger a_j \rangle_\rho$ , where  $\langle a_i^\dagger a_i \rangle_\rho = \text{tr}(\rho a_i^\dagger a_i)$ . However, if  $\rho$  is non-Gaussian we do not expect this equality to hold any more. We thus define the Wick's theorem violation as

$$\mathcal{W}(\rho) = |\langle a_i^\dagger a_i a_j^\dagger a_j \rangle_\rho - \langle a_i^\dagger a_i \rangle_\rho \langle a_j^\dagger a_j \rangle_\rho|, \quad (4)$$

which is a measure of how interacting a model is. In particular,  $\mathcal{W}(\rho)$  can be calculated with the use of the dominant entanglement spectrum levels [26]. It is possible to show that

$$\mathcal{W}(\rho) \leq \kappa D_{\mathcal{F}}(\rho), \quad (5)$$

where  $\kappa = 6$  for the case of the  $a_j$  and  $a_j^\dagger$  operators [26]. Hence, the interaction distance bounds from above the violation  $\mathcal{W}$  of Wick's theorem. When applied to the case of the XYZ model we find that  $\mathcal{W}$  and  $D_{\mathcal{F}}$  almost coincides throughout the phase diagram, as shown in Fig. 3(a).

The operators  $a_i$  and  $a_i^\dagger$  are, in general, related to  $c_j$  and  $c_j^\dagger$  of the underlying fermion lattice model (2) through a nonlinear and nonlocal transformation. Hence, in order to determine (4) experimentally, one needs full state tomography. As this is, in general, unrealistic to obtain in typical experiments, we

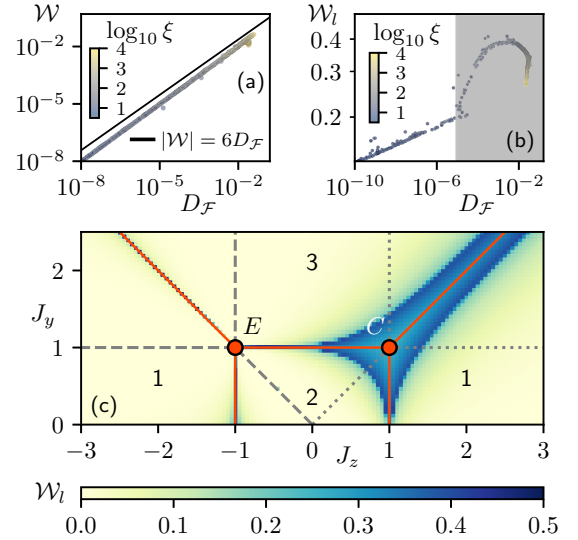


FIG. 3. (a) and (b) Scatterplots comparing  $|\mathcal{W}|$  in Eq. (4) and  $|\mathcal{W}_l|$  in Eq. (6) with  $D_{\mathcal{F}}$  for sizes  $L = 600$  and  $L = 400$ , respectively. We see that  $|\mathcal{W}|$  essentially coincides with  $D_{\mathcal{F}}$ , while  $|\mathcal{W}_l|$  strongly correlates with  $D_{\mathcal{F}}$  below the threshold  $D_{\mathcal{F}}^* \approx 10^{-9}$ . The shaded area,  $D_{\mathcal{F}} > D_{\mathcal{F}}^*$ , corresponds to data points near critical regions with high correlation lengths, where the relationship between  $D_{\mathcal{F}}$  and  $\mathcal{W}_l$  breaks down. (c)  $|\mathcal{W}_l|$  across the phase diagram of the XYZ model in Eq. (1) for size  $L = 400$ . When computing  $|\mathcal{W}_l|$ , we use a different Jordan-Wigner axis of quantization for each region, labeled as follows: in region 1 we pick the  $z$  quantization axis, in region 2 we pick the  $x$  axis, and in region 3 we pick the  $y$  axis.

apply the violation of Wick's theorem to the local operators  $c_j$  and  $c_j^\dagger$ . For convenience, we can employ the spin representation with the quantization axis taken to be the one for which the coefficient in the model is largest in absolute value, as shown in Fig. 3(c). For instance, where  $|J_z| \geq |J_y|$ ,  $|J_z|$  we define the violation of the local Wick's theorem as

$$\mathcal{W}_l(\rho) = |\langle Z_i Z_{i+1} \rangle_\rho - \langle Z_i \rangle_\rho \langle Z_{i+1} \rangle_\rho - \langle Y_i X_{i+1} \rangle_\rho \langle X_i Y_{i+1} \rangle_\rho + \langle X_i X_{i+1} \rangle_\rho \langle Y_i Y_{i+1} \rangle_\rho|, \quad (6)$$

which is given in terms of two-spin correlators that are experimentally accessible. While  $\mathcal{W}_l$  does not necessarily satisfy the inequality (5), we determined numerically that it is tightly related to  $D_{\mathcal{F}}$  with a monotonic one-to-one correspondence in the gapped region of the XYZ model, as shown in Fig. 3(b), where discrepancies from this behavior emerge only near the critical regions due to the finite-size effects. Thus,  $\mathcal{W}_l$  can successfully identify the emerging freedom of the XYZ model. In Fig. 3(c), we evaluated  $\mathcal{W}_l$  throughout the phase diagram of the XYZ model, finding behavior very similar to  $D_{\mathcal{F}}$  in Fig. 1(b).  $\mathcal{W}_l$  becomes identical to  $\mathcal{W}$  when the model is in the gapped antiferromagnetic phase of the XXZ model or when  $J_y^2 + J_z^2 \rightarrow \infty$  or  $J_y^2 + J_z^2 \rightarrow 0$ . Hence, the violation of the local Wick's theorem  $\mathcal{W}_l$  provides the same information as  $D_{\mathcal{F}}$ , while it can, in principle, be measured in the laboratory.

*Robustness under realistic conditions.* Finally, we consider the robustness of previous results when we move away from the exact XYZ model and introduce variations that model realistic experimental conditions. For example, in a cold-atom implementation, the interactions between the constituent

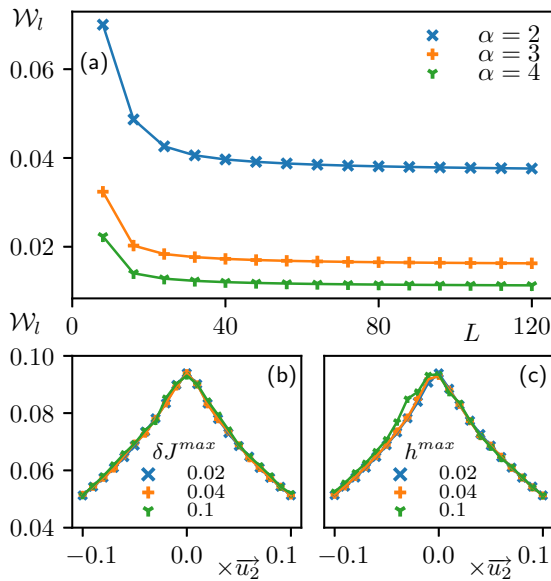


FIG. 4. (a)  $W_l$  as a function of system size for the long-range XYZ model in Eq. (7) with fixed  $J_x = -1.0$ ,  $J_y = -1.0$ , and  $J_z = 5.0$  and various  $\alpha$ . (b)  $W_l$  across the  $\vec{u}_2$  cut with different amounts of per site randomness  $\delta J^{\max}$  applied to the couplings  $J_x$ ,  $J_y$ , and  $J_z$  at system size  $L = 100$ . (c)  $W_l$  across the  $\vec{u}_2$  cut with a random local field of strength  $h^{\max}$  applied to every site of a  $L = 100$  system.

particles are characterized by a long-range algebraic decay [30,31]. Moreover, there might be inhomogeneities in the engineered couplings due to imperfections in the laser control procedures or spurious random local potentials.

We first consider the effect a polynomial profile of interactions has on the behavior of  $W_l$ . We introduce a long-range XYZ model,

$$H^{\text{LR}} = \sum_{i,n} \frac{1}{|i-n|^\alpha} (J_x X_i X_{i+n} + J_y Y_i Y_{i+n} + J_z Z_i Z_{i+n}), \quad (7)$$

where  $\alpha$  controls the power-law decay of the couplings. The ground-state properties of this model can be captured using finite DMRG by expressing the algebraically decaying interaction as a sum of exponentials in order to represent the Hamiltonian as a matrix-product operator [32,33]. In Fig. 4(a) we show the behavior of  $W_l$  as a function of system size in the long-range model. We picked a representative point which is in the gapped, antiferromagnetic phase for the entire range of  $\alpha$  values considered [34]. As in the short-range model,  $W_l$  decreases rapidly after the system exceeds a certain size  $L_{\min}$ . Note that, in contrast to the short-range case,  $W_l$  now levels off at a very small but nonzero value as  $L \rightarrow \infty$ , indicating that

the model does not become completely free in the thermodynamic limit. The saturation value depends on the couplings and  $\alpha$ .

A second type of robustness check we performed is the effect of experimental noise on  $W_l$ . To model this we first introduce randomized couplings on each site. In Fig. 4(b) the couplings along the  $\vec{u}_2$  cut are sampled uniformly from  $[J_i - \delta J^{\max}, J_i + \delta J^{\max}]$  on each site with  $W_l$  remaining stable and increasing only a small amount up to large variations in the couplings. We additionally consider the impact of a spurious local magnetic field in the  $z$  direction. In Fig. 4(c) a random local field sampled uniformly from  $[-h^{\max}, h^{\max}]$  was added on each site of the chain along the  $\vec{u}_2$  cut.  $W_l$  also shows stability under this class of perturbation. Hence, the emerging freedom of the XYZ model persists in the presence of experimental imperfections that break the integrability of the XYZ model in (2), while the behavior of its ground state correlations, as witnessed by  $D_{\mathcal{F}}$  and Wick's theorem violation, remains largely the same.

*Conclusions.* There is a stark contrast between the behavior of genuinely interacting systems and free ones in terms of their complexity in their description as well as their physical properties such as their thermalization and out-of-equilibrium dynamics. Baxter demonstrated that the XYZ model, which encompasses a large family of physically relevant models, behaves in the thermodynamic limit as free, although it incorporates fermionic interactions. Here, we identified the system size conditions for the freedom to emerge near and far away from the critical regions of the model as a function of the correlation length of the system. As our method does not rely on the integrability techniques, which are mainly restricted to one spatial dimension, it could be applied to other non-integrable 1D systems or even 2D models. Moreover, we quantified the emergent Gaussian behavior in the XYZ model for the experimentally relevant cases of finite system sizes, long-range interaction potentials, and inhomogeneous couplings and random local potentials. We proposed a way to observe the emergence of gaussianity in the correlations of the XYZ model in terms of observables that can be directly measured in the laboratory. As gaussianity emerges exponentially fast with system size, we anticipate that our findings can be experimentally verified in several experimental realizations of XYZ-type models, both in solid-state materials and in synthetic ultracold-atom systems [35–41].

In compliance with EPSRC policy framework on research data, this publication is theoretical work that does not require supporting research data.

*Acknowledgments.* We would like to thank F. Verstraete and C. Vlachou for inspiring conversations. This work was supported by EPSRC Grant No. EP/R020612/1.

- [1] I. Peschel and V. Eisler, Reduced density matrices and entanglement entropy in free lattice models, *J. Phys. A* **42**, 504003 (2009).
- [2] I. Affleck, T. Kennedy, E. H. Lieb, and H. Tasaki, Rigorous Results on Valence-Bond Ground States in Antiferromagnets, *Phys. Rev. Lett.* **59**, 799 (1987).

- [3] R. B. Laughlin, Anomalous Quantum Hall Effect: An Incompressible Quantum Fluid with Fractionally Charged Excitations, *Phys. Rev. Lett.* **50**, 1395 (1983).
- [4] T. Giamarchi and O. U. Press, *Quantum Physics in One Dimension*, International Series of Monographs on Physics (Clarendon, Oxford, 2004).

- [5] T. Schweigler, M. Gluza, M. Tajik, S. Sotiriadis, F. Cataldini, S.-C. Ji, F. S. Møller, J. Sabino, B. Rauer, J. Eisert, and J. Schmiedmayer, Decay and recurrence of non-Gaussian correlations in a quantum many-body system, *Nat. Phys.* **17**, 559 (2021).
- [6] B. Sutherland, Two-dimensional hydrogen bonded crystals without the ice rule, *J. Math. Phys.* **11**, 3183 (1970).
- [7] R. J. Baxter, One-Dimensional Anisotropic Heisenberg Chain, *Phys. Rev. Lett.* **26**, 834 (1971).
- [8] R. J. Baxter, Eight-Vertex Model in Lattice Statistics, *Phys. Rev. Lett.* **26**, 832 (1971).
- [9] R. J. Baxter, *Exactly Solved Models in Statistical Mechanics* (Academic, London, 1985), pp. 5–63.
- [10] R. Baxter, Eight-vertex model in lattice statistics and one-dimensional anisotropic Heisenberg chain. III. Eigenvectors of the transfer matrix and Hamiltonian, *Ann. Phys. (NY)* **76**, 48 (1973).
- [11] T. Nishino, Density matrix renormalization group method for 2D classical models, *J. Phys. Soc. Jpn.* **64**, 3598 (1995).
- [12] T. Nishino and K. Okunishi, Corner transfer matrix algorithm for classical renormalization group, *J. Phys. Soc. Jpn.* **66**, 3040 (1997).
- [13] L. A. Takhtadzhian and L. D. Faddeev, The quantum method of the inverse problem and the Heisenberg XYZ model, *Russ. Math. Surv.* **34**, 11 (1979).
- [14] I. Peschel, M. Kaulke, and Ö. Legeza, Density-matrix spectra for integrable models, *Ann. Phys. (Berlin, Ger.)* **8**, 153 (1999).
- [15] A. Roy, D. Schuricht, J. Hauschild, F. Pollmann, and H. Saleur, The quantum sine-Gordon model with quantum circuits, *Nucl. Phys. B* **968**, 115445 (2021).
- [16] M. E. Peskin and D. V. Schroeder, *An Introduction to Quantum Field Theory* (Addison-Wesley, Reading, MA, 1995).
- [17] C. J. Turner, K. Meichanetzidis, Z. Papić, and J. K. Pachos, Optimal free descriptions of many-body theories, *Nat. Commun.* **8**, 14926 (2017).
- [18] J. K. Pachos and Z. Papić, Quantifying the effect of interactions in quantum many-body systems, *SciPost Phys. Lect. Notes* **4** (2018).
- [19] K. Patrick, V. Caudrelier, Z. Papić, and J. K. Pachos, Interaction distance in the extended XXZ model, *Phys. Rev. B* **100**, 235128 (2019).
- [20] E. Lieb, T. Schultz, and D. Mattis, Two soluble models of an antiferromagnetic chain, *Ann. Phys. (NY)* **16**, 407 (1961).
- [21] E. Ercolessi, S. Evangelisti, F. Franchini, and F. Ravanini, Essential singularity in the Renyi entanglement entropy of the one-dimensional XYZ spin- $\frac{1}{2}$  chain, *Phys. Rev. B* **83**, 012402 (2011).
- [22] H. Li and F. D. M. Haldane, Entanglement Spectrum as a Generalization of Entanglement Entropy: Identification of Topological Order in Non-Abelian Fractional Quantum Hall Effect States, *Phys. Rev. Lett.* **101**, 010504 (2008).
- [23] D. Markham, J. A. Miszczak, Z. Puchała, and K. Życzkowski, Quantum state discrimination: A geometric approach, *Phys. Rev. A* **77**, 042111 (2008).
- [24] S. R. White, Density Matrix Formulation for Quantum Renormalization Groups, *Phys. Rev. Lett.* **69**, 2863 (1992).
- [25] M. Fishman, S. R. White, and E. M. Stoudenmire, The ITensor software library for tensor network calculations, [arXiv:2007.14822](https://arxiv.org/abs/2007.14822).
- [26] See Supplemental Material at <http://link.aps.org/supplemental/10.1103/PhysRevB.104.L180408> for the value of the correlation length of the XYZ model throughout the phase diagram.
- [27] H. Pichler, G. Zhu, A. Seif, P. Zoller, and M. Hafezi, Measurement Protocol for the Entanglement Spectrum of Cold Atoms, *Phys. Rev. X* **6**, 041033 (2016).
- [28] M. Dalmonte, B. Vermersch, and P. Zoller, Quantum simulation and spectroscopy of entanglement Hamiltonians, *Nat. Phys.* **14**, 827 (2018).
- [29] C. Kokail, R. van Bijnen, A. Elben, B. Vermersch, and P. Zoller, Entanglement Hamiltonian tomography in quantum simulation, *Nat. Phys.* **17**, 936 (2021).
- [30] L. D. Carr, D. DeMille, R. V. Krems, and J. Ye, Cold and ultracold molecules: Science, technology and applications, *New J. Phys.* **11**, 055049 (2009).
- [31] A. Mazurenko, C. S. Chiu, G. Ji, M. F. Parsons, M. Kanász-Nagy, R. Schmidt, F. Grusdt, E. Demler, D. Greif, and M. Greiner, A cold-atom Fermi–Hubbard antiferromagnet, *Nature (London)* **545**, 462 (2017).
- [32] B. Pirvu, V. Murg, J. I. Cirac, and F. Verstraete, Matrix product operator representations, *New J. Phys.* **12**, 025012 (2010).
- [33] M. J. O’Rourke, Z. Li, and G. K.-L. Chan, Efficient representation of long-range interactions in tensor network algorithms, *Phys. Rev. B* **98**, 205127 (2018).
- [34] M. F. Maghrebi, Z.-X. Gong, and A. V. Gorshkov, Continuous Symmetry Breaking in 1D Long-Range Interacting Quantum Systems, *Phys. Rev. Lett.* **119**, 023001 (2017).
- [35] F. Pinheiro, G. M. Bruun, J.-P. Martikainen, and J. Larson, XYZ Quantum Heisenberg Models with  $p$ -Orbital Bosons, *Phys. Rev. Lett.* **111**, 205302 (2013).
- [36] G. Pelegrí, J. Mompart, V. Ahufinger, and A. J. Daley, Quantum magnetism with ultracold bosons carrying orbital angular momentum, *Phys. Rev. A* **100**, 023615 (2019).
- [37] L. Tarruell and L. Sanchez-Palencia, Quantum simulation of the Hubbard model with ultracold fermions in optical lattices, *C. R. Phys.* **19**, 365 (2018).
- [38] P. N. Jepsen, J. Amato-Grill, I. Dimitrova, W. W. Ho, E. Demler, and W. Ketterle, Spin transport in a tunable Heisenberg model realized with ultracold atoms, *Nature (London)* **588**, 403 (2020).
- [39] A. Scheie, N. E. Sherman, M. Dupont, S. E. Nagler, M. B. Stone, G. E. Granroth, J. E. Moore, and D. A. Tennant, Detection of Kardar–Parisi–Zhang hydrodynamics in a quantum Heisenberg spin- $\frac{1}{2}$  chain, *Nat. Phys.* **17**, 726 (2021).
- [40] M. Gring, M. Kuhnert, T. Langen, T. Kitagawa, B. Rauer, M. Schreitl, I. Mazets, D. A. Smith, E. Demler, and J. Schmiedmayer, Relaxation and prethermalization in an isolated quantum system, *Science* **337**, 1318 (2012).
- [41] S. Murmann, F. Deuretzbacher, G. Zürn, J. Bjerlin, S. M. Reimann, L. Santos, T. Lompe, and S. Jochim, Antiferromagnetic Heisenberg Spin Chain of a Few Cold Atoms in a One-Dimensional Trap, *Phys. Rev. Lett.* **115**, 215301 (2015).